Asian Journal of Chemistry; Vol. 26, No. 6 (2014), 1869-1872

ASIAN JOURNAL OF CHEMISTRY

http://dx.doi.org/10.14233/ajchem.2014.16520

Cyclic Microwave-Assisted Metathetic Synthesis of SPION/ $Ca_3V_2O_8:Er^{3+},Yb^{3+}$ Nanocomposites and Their Optical Properties

CHANG SUNG LIM

Department of Advanced Materials Science & Engineering, Hanseo University, Seosan 356-706, Republic of Korea

Corresponding author: Tel/Fax: +82 41 6601445; E-mail: cslim@hanseo.ac.kr

Received: 14 October 2013; *Accepted*: 28 February 2014; *Published online*: 10 March 2014; AJC-14919

Er^{3+}/Yb^{3+} co-doped $Ca_3V_2O_8$ ($Ca_3V_2O_8:Er^{3+}/Yb^{3+}$) nanocomposites with superparamagnetic iron oxide nanoparticles (SPIONs) have been successfully synthesized by a cyclic microwave-assisted metathetic method followed by heat-treatment. The microstructure exhibited well-defined and homogeneous morphology with the $Ca_3V_2O_8:Er^{3+}/Yb^{3+}$ particle size of 1-2 μm and Fe_3O_4 particle size of 100-500 nm. The Fe_3O_4 nonoparticles were self-preferentially crystallized and immobilized on the surface of $Ca_3V_2O_8:Er^{3+}/Yb^{3+}$ particles. The synthesized SPION/$Ca_3V_2O_8:Er^{3+}/Yb^{3+}$ nanocomposites were characterized by X-ray diffraction, scanning electron microscopy and energy-dispersive X-ray spectroscopy. Other optical properties were also examined using photoluminescence emission measurements and Raman spectroscopy.

Keywords: Cyclic microwave-assisted metathetic synthesis, Optical properties, SPION/$Ca_3V_2O_8:Er^{3+}/Yb^{3+}$, Nanocomposites.

INTRODUCTION

Multifunctional nanocomposites that exhibit significant magnetic moment and luminescence have attracted much attention because of various applications in biotechnology, medicine and quality inspection. The superparamagnetic iron oxide nanoparticles (SPIONs) incorporated into photoluminescent composites containing two different functionalities could provide novel characteristics *via* the integration of fluorescent and magnetic properties, offering new potential in a wide range of applications in biomedical systems, such as targeted drugs, diagnostics, therapeutics and bio-imaging[1-3]. The metal orthovanadates have been developed to enhance the applications of metal orthovanadate prepared by a range of processes, such as a solid-state reaction[4,5], the solution phase metathetic method[6], the sol-gel[7], the solid-state metathesis approach[8], the mechano-chemical method[9] and the floating zone technique[10]. Among different methods, solution-based chemical synthetic methods play the key role in the design and production of fine oxide powders and are successful in overcoming many limitations of traditional solid-state, high-temperature methods. The microwave heating is delivered to the surface of the material by radiant and/or convection heating, which is transferred to the bulk of the material *via* conduction. So, the microwave energy is delivered directly to the material through the molecular interactions with electromagnetic field. Heat can be generated through volumetric heating because microwaves can penetrate the material and supply energy[11-14].

The cyclic microwave-assisted metathetic (MAM) synthesis of materials is a simple and cost-effective method that provides a high yield with an easy scale-up and it is emerging as a viable alternative approach for the synthesis of high-quality novel inorganic materials in short time periods[15,16]. In the present study, the Er^{3+}/Yb^{3+} co-doped $Ca_3V_2O_8$ ($Ca_3V_2O_8:Er^{3+}/Yb^{3+}$) and Er^{3+}/Yb^{3+} co-doped $Ca_3V_2O_8$ with SPIONs (SPION/$Ca_3V_2O_8:Er^{3+}/Yb^{3+}$) nanocomposites were synthesized by the cyclic MAM method followed by heat-treatment. The synthesized $Ca_3V_2O_8:Er^{3+}/Yb^{3+}$and SPION/$Ca_3V_2O_8:Er^{3+},Yb^{3+}$ nanocomposites were characterized by X-ray diffraction (XRD), scanning electron microscopy (SEM) and energy-dispersive X-ray spectroscopy (EDS). Spectroscopic properties have been investigated by photoluminescence emission measurements and Raman spectroscopy.

EXPERIMENTAL

Appropriate stoichiometric amounts of $CaCl_2$, $ErCl_3·6H_2O$, $YbCl_3·6H_2O$, Na_3VO_4, 5-nm-sized Fe_3O_4 nanoparticles and ethylene glycol of analytical reagent grade were used to prepare the $Ca_3V_2O_8:Er^{3+},Yb^{3+}$ and SPION/$Ca_3V_2O_8:Er^{3+},Yb^{3+}$ compounds. To prepare $Ca_3V_2O_8:Er^{3+}/Yb^{3+}$, 0.8 mol% $CaCl_2$ with 0.02 mol % $ErCl_3·6H_2O$ and 0.18 mol % $YbCl_3·6H_2O$ and 1 mol % Na_3VO_4 were dissolved in 30 mL of ethylene glycol. To prepare SPION/$Ca_3V_2O_8:Er^{3+},Yb^{3+}$, 0.2 mol% $CaCl_2$ with 0.02 mol % $ErCl_3·6H_2O$ and 0.18 mol% $YbCl_3·6H_2O$ and 1 mol % Na_3VO_4 with 0.5 mol % Fe_3O_4 were dissolved in 30 mL ethylene glycol. The solutions were mixed and adjusted to pH

9.5 using NaOH. The solutions were stirred at room temperature. Then, the mixtures were transferred into 120 mL Teflon vessels. Each Teflon vessel was placed into a microwave oven operating at the frequency of 2.45 GHz with the maximum output power of 1250 W for 23 min. The working cycle of the MAM reaction was been controlled precisely between 30 s on and 30 s off for 8 min, followed by a further treatment of 30 s on and 60 s off for 15 min. Ethylene glycol was evaporated slowly at its boiling point. Ethylene glycol is a polar solvent at its boiling point of 197 °C and it is a good candidate for the microwave process. The resulted powder samples were treated with ultrasonic radiation and washed many times with hot distilled water. The white precipitates were collected and dried at 100 °C in a drying oven. After this, the final products were heat-treated at 600 °C for 3 h.

The phase composition of final powder products formed after the cyclic MAM reaction and following heat-treatment was identified using XRD (D/MAX 2200, Rigaku, Japan). The microstructures and surface morphologies of the $Ca_3V_2O_8$:Er^{3+}/Yb^{3+} and SPION/ $Ca_3V_2O_8$:Er^{3+}/Yb^{3+} nanocomposites were observed using SEM/EDS (JSM-5600, JEOL, Japan). Their photoluminescence spectrum was recorded at room temperature using a spectrophotometer (Perkin Elmer LS55, UK). Raman spectroscopy measurements were performed using a LabRam HR (Jobin-Yvon, France) device. The 514.5-nm line of an Ar-ion laser was used as an excitation source and the power on the samples was kept at 0.5 mW.

RESULTS AND DISCUSSION

Fig. 1 shows the XRD pattern of the synthesized SPION/$Ca_3V_2O_8$:Er^{3+}/Yb^{3+} nanocomposites. All the observed diffraction peaks can be assigned to the trigonal-phase $Ca_3V_2O_8$ (space group *R3c*) and Fe_3O_4, which were in good agreement with the crystallographic data of $Ca_3V_2O_8$ (JCPDS: 46-756) and Fe_3O_4 (JCPDS 19-0629). The diffraction peaks marked with asterisk are related to Fe_3O_4. The result confirms that the SPION/$Ca_3V_2O_8$:Er^{3+},Yb^{3+} nanocomposites can be prepared using the cyclic MAM route. The post-synthesis heat-treatment plays an important role in forming well-defined crystallized micromorphology. To achieve such morphology, the SPION/$Ca_3V_2O_8$:Er^{3+},Yb^{3+} nanocomposites need to be heated at 600 °C for 3 h. This suggests that the cyclic MAM route, in combination with subsequent heat-treatment, is a suitable way for the formation of SPION/$Ca_3V_2O_8$:Er^{3+},Yb^{3+} nanocomposites with well developed high-intensity peaks from the at (210) planes, which are the major peaks of $Ca_3V_2O_8$.

The SEM image of the synthesized SPION/$Ca_3V_2O_8$:Er^{3+}, Yb^{3+} nanocomposite is shown in Fig. 2. The as-synthesized sample has a well-defined and homogeneous with the particle size of the $Ca_3V_2O_8$:Er^{3+},Yb^{3+} in the range of 1-2 μm and Fe_3O_4 in the range of 100-500 nm, respectively. The Fe_3O_4 nanoparticles were self-preferentially crystallized and immobilized on the surface of big $Ca_3V_2O_8$:Er^{3+},Yb^{3+} particles. The incorporation of Fe_3O_4 nanoparticles to the $Ca_3V_2O_8$:Er^{3+},Yb^{3+} compound particles can be successfully achieved using the cyclic MAM. The MAM reactions, such as $3CaCl_2 + 2Na_3VO_4 \rightarrow Ca_3V_2O_8 + 6NaCl$, involve the exchange of atomic/ionic species, in which the driving force is the exothermic reaction

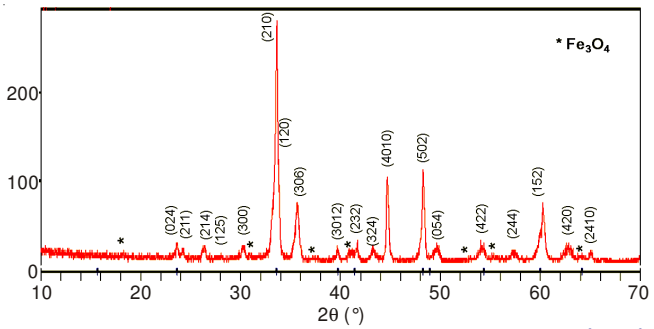

Fig. 1. XRD pattern of the synthesized SPION/$Ca_3V_2O_8$:Er^{3+}/Yb^{3+} nanocomposites

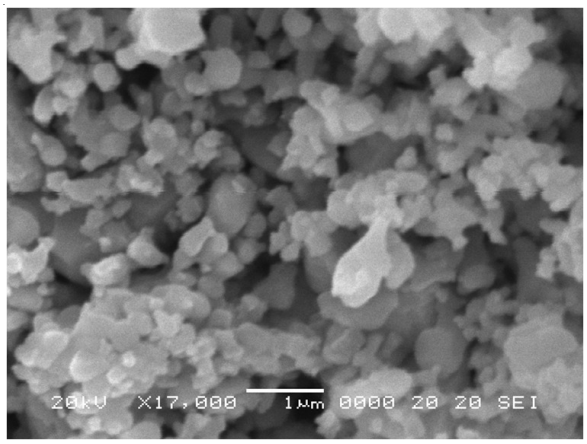

Fig. 2. SEM images of the synthesized (a) SPION/$Ca_3V_2O_8$:Er^{3+},Yb^{3+} nanocomposite and (b) high-magnification

accompanying the formation of NaCl[16]. The SPION/$Ca_3V_2O_8$:Er^{3+},Yb^{3+} nanocomposites were heated rapidly and uniformly by the cyclic MAM route. This classifies the method among simple and cost-effective ones and, evidently, the MAM technology is able to provide high yields with an easy scale-up as a viable alternative for the rapid synthesis of complex oxide composites[16].

The EDS pattern, quantitative compositions, quantitative results and the SEM image of the synthesized SPION/$Ca_3V_2O_8$:Er^{3+},Yb^{3+} nanocomposite are presented in Fig. 3. The EDS pattern shown in Fig. 3(a) displays that the SPION/$Ca_3V_2O_8$:Er^{3+},Yb^{3+} sample is composed of Fe, Ca, V, O, Er and Yb with the dominance of Fe, Ca, V, O. The EDS pattern and quantitative compositions in Fig. 3(a, b) could be well assigned to the SPION/$Ca_3V_2O_8$:Er^{3+},Yb^{3+} composite. Thus, the incorporation of Fe_3O_4 nanoparticles to the SPION/$Ca_3V_2O_8$:Er^{3+},Yb^{3+} compound particles can be successfully achieved using the cyclic MAM. The cyclic MAM reactions provide a convenient route for the synthesis of such complex products as SPION/$Ca_3V_2O_8$:Er^{3+},Yb^{3+} composites. The cyclic MAM route provides the exothermic energy to synthesize the bulk of the material uniformly, so that fine particles with controlled morphology can be fabricated in an environmentally friendly manner and without solvent waste generation.

The photoluminescence emission spectrum of the synthesized SPION/$Ca_3V_2O_8$:Er^{3+},Yb^{3+} nanocomposite excited at 250 nm at room temperature is shown in Fig. 4. It is generally assumed that the measured emission spectrum of metal orthovanadates are mainly due to charge-transfer transitions

(a)

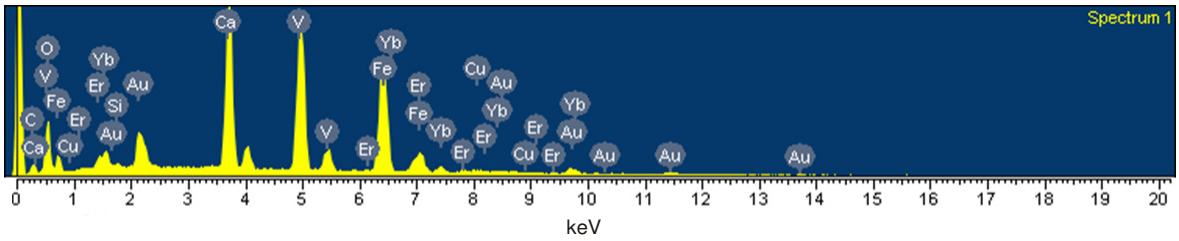

(b)

Spectrum	In stats.	C	O	Si	Ca	V	Fe	Cu	Er	Yb	Total
Spectrum 1	Yes	7.05	32.65	0.22	11.63	16.65	21.17	1.13	5.12	4.38	100.00
Mean		7.05	32.65	0.22	11.63	16.65	21.17	1.13	5.12	4.38	100.00
Std. deviation		0.00	0.00	0.00	0.00	0.00	0.00	0.00	0.00	0.00	
Max.		7.05	32.65	0.22	11.63	16.65	21.17	1.13	5.12	4.38	
Min.		7.05	32.65	0.22	11.63	16.65	21.17	1.13	5.12	4.38	

(c)

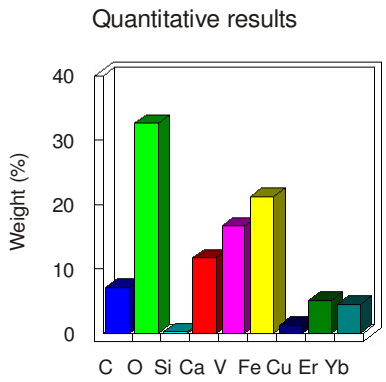

(d)

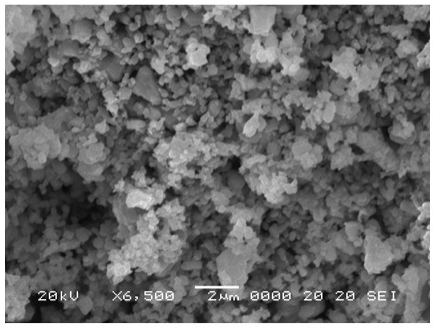

Fig. 3. (a) EDS pattern, (b) quantitative compositions, (c) quantitative results and (d) SEM image of the synthesized SPION/$Ca_3V_2O_8$: Er^{3+},Yb^{3+} nanocomposites

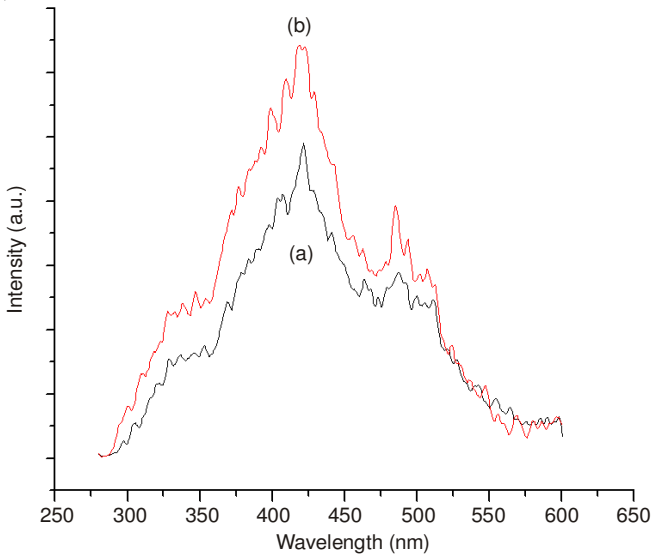

Fig. 4. Photoluminescence emission spectrum of the synthesized SPION/$Ca_3V_2O_8$:Er^{3+},Yb^{3+} composite excited at 250 nm at room temperature

within the $[VO_4]^{3-}$ complex. With excitation at 250 nm, the spectrum of the nanocomposites exhibit major photoluminescence emissions in the blue wavelength range of 420-430 nm. The emissions of four narrow shoulders at approximately 490, 510, 530 and 530 nm are considered to form by defect structures. The emission spectra of metal orthovanadates are due mainly to charge-transfer transitions within the $[VO_4]^{3-}$ complex. The explanation of the narrow shoulders in Fig. 5 is proposed considering the Jahn-Teller splitting effect[17,18] on excited states of $[VO_4]^{3-}$ and anion in the $Ca_3V_2O_8$. This is similar to that reported by Zhang *et al.*[19]. The Jahn-Teller splitting effect essentially determines the emission shape of the $Ca_3V_2O_8$ particles. The additional emission bands can be interpreted by the existence of Frenkel defect structures (oxygen ion shifted to the inter-position with the simultaneous creation of vacancies) in the surface layers of the $Ca_3V_2O_8$ particles[20,21].

Fig. 5 shows the Raman spectra of the synthesized (A) $Ca_3V_2O_8$ particles and (B) $Ca_3V_2O_8$:Er^{3+},Yb^{3+} (CVO:ErYb) and SPION/$Ca_3V_2O_8$:Er^{3+},Yb^{3+} (F-CVO:ErYb) nanocomposites excited by the 514.5-nm line of an Ar-ion laser at 0.5 mW. The Raman modes for the $Ca_3V_2O_8$ particles in Fig. 5(A) were detected as $\nu_1(A_g)$, $\nu_3(B_g)$, $\nu_3(E_g)$, $\nu_4(E_g)$, $\nu_4(B_g)$ and $\nu_2(B_g)$ vibrations at 873, 716, 490 and 342 cm^{-1}, the free rotation modes were detected at 277-257 cm^{-1} and the external mode was localized at 156 and 133 cm^{-1}. The well-resolved sharp peaks for the $Ca_3V_2O_8$ nanoparticles indicate that the synthesized particles are highly crystallized. The vibration modes in the Raman spectrum of $Ca_3V_2O_8$ nanoparticles are classified into two groups, internal and external[22,23]. The internal

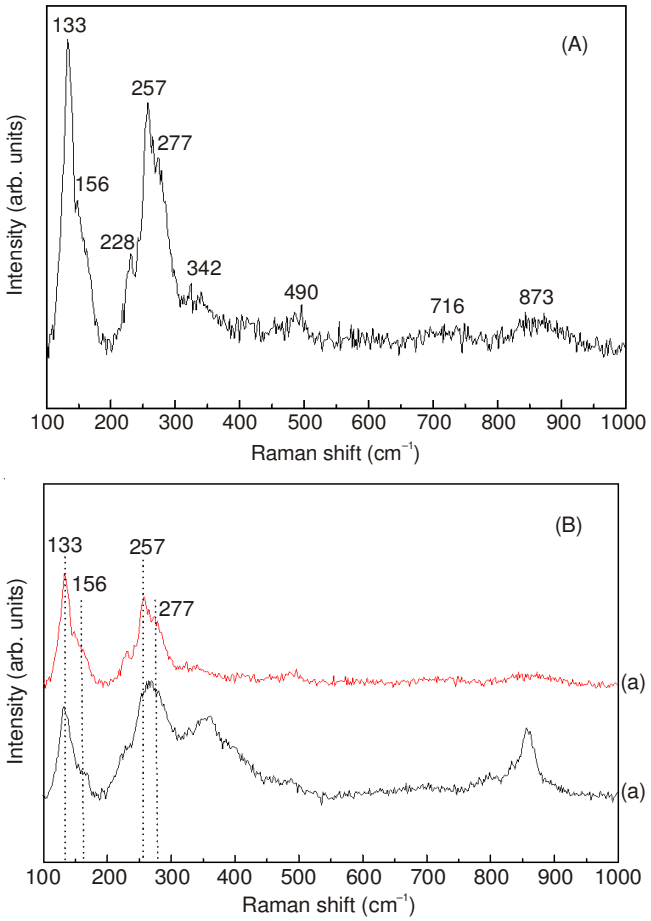

Fig. 5. Raman spectra of the synthesized (A) $Ca_3V_2O_8$ particles and (B) $Ca_3V_2O_8$:Er^{3+},Yb^{3+} (CVO:ErYb) and SPION/$Ca_3V_2O_8$:Er^{3+},Yb^{3+}(F-CVO:ErYb) nanocomposites

vibrations are related to the $[VO_4]^{3-}$ molecular group with a stationary mass center. The external vibrations or lattice phonons are associated to the motion of the Ca^{2+} cation and rigid molecular units. The type of cations (Ca^{2+}, Sr^{2+}, Ba^{2+}) can influence on the Raman modes by changing the size of the crystal unit cell and by covalent cation effect[23]. The internal modes for the $Ca_3V_2O_8$:Er^{3+},Yb^{3+}(CVO:ErYb) composites in Fig. 5(B) were detected at 873, 716, 490 and 342 cm^{-1}, the free rotation modes were detected at 277-257 cm^{-1} and the external mode was localized at 156 and 133 cm^{-1}. However, the Raman modes of SPION/$Ca_3V_2O_8$:Er^{3+},Yb^{3+}(F-CVO:ErYb) indicate very lower than those of $Ca_3V_2O_8$ and $Ca_3V_2O_8$:Er^{3+},Yb^{3+}(CVO:ErYb).

The internal vibration mode frequencies are dependent on the lattice parameters and the degree of the partially covalent bonding between the cations and molecular ionic group[23] $[VO_4]^{3-}$. It is noted that the Fe_3O_4 particles have no influence on the Raman spectra, while the doping ion of Er^{3+}/Yb^{3+} can influence the Raman spectra. The Raman spectra proved that the Er^{3+}/Yb^{3+} doping ions can influence the structure of the host materials.

Conclusion

The nanocomposites of SPION/$Ca_3V_2O_8$:Er^{3+},Yb^{3+} were successfully synthesized by a cyclic MAM method. The microstructure exhibited a well-defined and homogeneous morphology with the $Ca_3V_2O_8$:Er^{3+},Yb^{3+} and Fe_3O_4 particle size of 1-2 μm and 100-500 nm, respectively. The Fe_3O_4 nanoparticles were self-preferentially crystallized and immobilized on the surface of $Ca_3V_2O_8$:Er^{3+},Yb^{3+} particles. The Raman modes of SPION/$Ca_3V_2O_8$:Er^{3+},Yb^{3+} (F-CVO:ErYb) indicate very lower than those of $Ca_3V_2O_8$ and $Ca_3V_2O_8$:Er^{3+},Yb^{3+} (CVO:ErYb). The Fe_3O_4 particles have no influence on the Raman spectra, while the doping ion of Er^{3+}/Yb^{3+} can influence the Raman spectra. The Raman spectra proved that the Er^{3+}/Yb^{3+} doping ions can influence the structure of the host materials.

ACKNOWLEDGEMENTS

This study was supported by Basic Science Research Program through the National Research Foundation of Korea (NRF) funded by the Ministry of Education, Science and Technology (2013-054508).

REFERENCES

1. D. Liu, L. Tong, J. Shi and H. Yang, *J. Alloys Comp*., **512**, 361 (2012).
2. L. Liu, L. Xiao and H.Y. Zhu, *Chem. Phys. Lett.,* **539-540**, 112 (2012).
3. Q. Wang, X. Yang, L. Yu and H. Yang, *J. Alloys Comp.*, **509**, 9098 (2011).
4. D. Wang, Z. Zou and J. Ye, Res. *Chem. Intermed*., **31**, 433 (2005).
5. M. Kurzawa and A. Blonska-Tabero, *J. Therm. Anal. Calorim*., **77**, 17 (2004).
6. P. Parhi and V. Manivannan, *Mater. Res. Bull*. **43**, 2966 (2008).
7. S.S. Kim, H. Ikuta and M. Wakihara, *Solid State Ion.* **139**, 57 (2001).
8. P. Parhi, V. Manivannan, S. Kohli and P. Mccurdy, *Bull. Mater. Sci*., **31**, 885 (2008).
9. V. Manivannan, P. Parhi and J. Howard, *J. Cryst. Growth*, **310**, 2793 (2008).
10. R. Szymczak, M. Baran, J. Fink-Finowicki, B. Krzymanska, P. Aleshkevych, H. Szymczak, S.N. Barilo, G.L. Bychkov and S.V. Shiryaev, *J. Non-Cryst. Solids*, **354**, 4186 (2008).
11. T. Trongtem, A. Phuruangrat and S. Trongtem, *J. Nanopart. Res.*, **12**, 2287 (2010).
12. C.S. Lim, *Mater. Res. Bull*., **47**, 4220 (2012).
13. C.S. Lim, *Asian J. Chem*., **25**, 63 (2013).
14. S. Das, A.K. Mukhopadhyay, S. Datta and D. Basu, *Bull. Mater. Sci*., **32**, 1 (2009).
15. C.S. Lim, *J. Lumin*., **132**, 1774 (2012).
16. C.S. Lim, *Mater. Chem. Phys*., **131**, 714 (2012).
17. Y. Toyozawa and M. Inoue, *J. Phys. Soc. Jpn*., **21**, 1663 (1966).
18. E.G. Reut, *Izv. Akad. Nauk SSSR, Ser. Fiz*., **43**, 1186 (1979).
19. Y. Zhang, N.A.W. Holzwarth and R.T. Williams, *Phys. Rev. B*, **57**, 12738 (1998).
20. J. Van Tol, *Mol. Phys*., **88**, 803 (1996).
21. V.B. Mikhailik, H. Kraus, D. Wahl and M.S. Mykhaylyk, *Phys. Status Solid B*, **242**, R17 (2005).
22. T.T. Basiev, A.A. Sobol, Y.K. Voronko and P.G. Zverev, *Opt. Mater*., **15**, 205 (2000).
23. T.T. Basiev, A.A. Sobol, P.G. Zverev, L.I. Ivleva, V.V. Osiko and R.C. Powell, *Opt. Mater*., **11**, 307 (1997).